Electrochemistry Communications 117 (2020) 106780

Contents lists available at ScienceDirect

Electrochemistry Communications

journal homepage: www.elsevier.com/locate/elecom

Facile visualization of the initial nucleation and growth of an active metal electrodeposited in a high temperature molten salt using a detachable disk electrode

Kui Liu[a], Yue Ma[a], Mingliang Kang[a,*], Biao Wang[a,b,*]

[a] Sino-French Institute of Nuclear Engineering and Technology, Sun Yat-sen University, Zhuhai 519000, China
[b] School of Physics, Sun Yat-sen University, Guangzhou 510275, China

ARTICLE INFO

Keywords:
Detachable disk electrode
Initial nucleation and growth morphology
High temperature molten salt
Uranium

ABSTRACT

In molten salt electrodeposition, a clear understanding of the initial nucleation and growth of nuclei formed on a substrate/electrode is critical to determining the morphology and structure of deposits in order to produce devices and products in various scientific fields. However, it is a challenge to obtain and characterize micro- or nano-sized nuclei, especially for very active elements due to their high sensitivity to water and oxygen. This problem is made even worse when the nuclei are accompanied by a larger amount of solid salts. In this work, we have designed a detachable disk electrode (DDE) which can prevent inessential salts from adhering to the disk substrate, greatly reducing the operational complexity, and ultimately enhancing the effectiveness and ease of visualizing initial nucleation. Uranium, a typical radioactive element with high metallic activity in the nuclear fuel cycle, was chosen as an example to test the sampling performance of the DDE. High-quality visualization of the initial nucleation and growth morphology of uranium on different substrates is presented here for the first time. The DDE provides a universal and simple scheme with wide applicability to the study of initial nucleation in high temperature molten salts, in fields such as electrodeposition, electrosynthesis, electroplating, etc.

1. Introduction

Molten salts possessing a high dissolution capacity, chemical stability and reactivity and relatively low vapor tension have applications in many industrial processes [1,2], such as the classical Hall-Héroult process for aluminium production [3], electrocoating [4] and electropolishing [5], electrosynthesis of functional materials [6], electrowinning and electrorefining of refractory metals [7,8] and spent nuclear fuels (SNF) in pyrochemical reprocessing [9–11], etc. Therefore, a good understanding of the chemical and physical properties involved in these processes is essential for practical operation, maintenance and technical upgrades. A variety of analytical methods and techniques have been used to help understand the molten salt solvents, species, chemical and electrochemical mechanisms/processes, including absorption [9,12–14] and scattering [15,16] spectroscopy, spectroelectrochemistry [13,17], macro [18,19] and micro [1,20] electrodes, in situ [21] and ex situ [22] monitoring techniques, etc.

Among the industrial applications involving high temperature molten salts (HTMS), the most obvious one is electrodeposition/electrolysis. The very early stages of nucleation and growth of nuclei on a substrate/electrode are critical in determining the morphology and structure of the deposits, when the aim is often to achieve stable electrodeposition. Increasing attention [18,23–27] has been paid to the performance of metals in this step in HTMS. However, most of these works have been restricted to explaining the fundamental nucleation mechanism using electrochemical methods such as chronoamperometry [28]. The evolution of the morphology and growth of nuclei at early stages of electrocrystallization in HTMS, which is crucial for subsequent deposition, is still not well understood, especially for active metallic elements such as actinides and lanthanides.

However, it is very difficult to obtain samples of early stage nuclei. Early crystal nuclei are generally deposited instantaneously, therefore the sample is very small. In addition, micro- or nano-sized nuclei are very sensitive to water and oxygen, and electrodeposition is generally accompanied by larger amounts of solid salts. Thus, it is problematic to obtain the initial nuclei without alteration if cleaning with water or an organic solvent. To avoid the adhesion of a molten salt, Pesic et al. reported the straightforward and smart idea of preparing a Mo disk electrode from a side-shielded 3 mm width × 10 mm length Mo cylinder [18]. They found that a fresh and well-polished Mo surface did

---

* Corresponding authors.
E-mail addresses: kangml3@mail.sysu.edu.cn (M. Kang), wangbiao@mail.sysu.edu.cn (B. Wang).

https://doi.org/10.1016/j.elecom.2020.106780
Received 26 May 2020; Received in revised form 20 June 2020; Accepted 20 June 2020

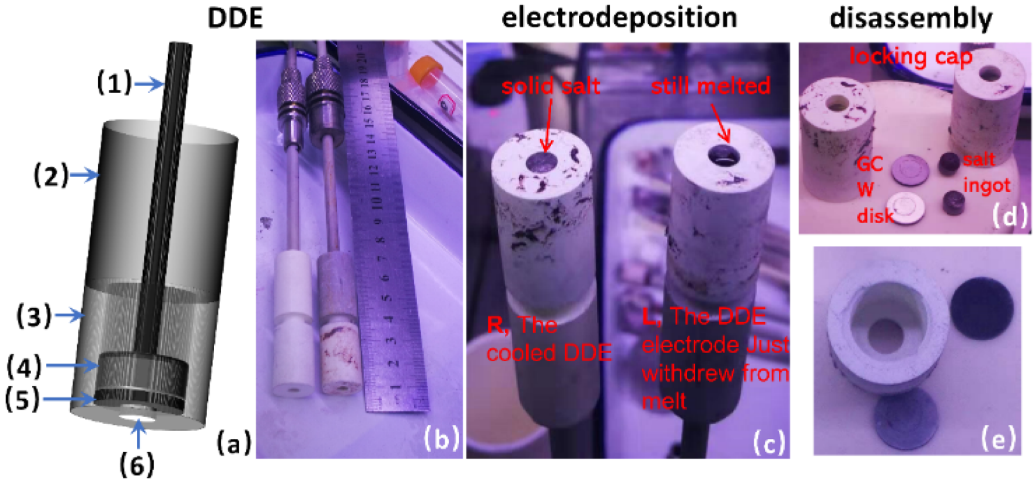

Fig. 1. (a) Schematic diagram of the DDE: (1) STS current collector, (2–3) BN fastening screw rod and nut, (4) STS top fastener, (5) disk, (6) working hole. (b) The DDE. (c) The DDE after withdrawal from a molten salt containing uranium (left, cooled; right, just withdrawn). (d) The locking cap (nut), GC and W disks and the removed cylindrical solidified salt. (e) Inner side of the nut after withdrawal.

not retain molten salt upon withdrawal and yielded high-quality SEM images of the initial formation and growth of nuclei of several lanthanide elements in molten salt electrolysis [18,29]. However, due to the large size and complex shielding of the electrode, a special sample stage had to be designed before attempting the electron microscopy studies.

In this work, we have designed a detachable disk electrode (DDE) in order to characterize the initial formation and growth of nuclei in HTMS electrolysis. Our design makes it possible to easily replace the disk substrate with different materials, which in turn helps to reduce the complexity of the experiments and enhance the efficiency of HTMS electroanalysis. Using the DDE, high-quality samples of early nucleation on different substrates can be obtained for optimized characterization and analysis of metal electrocrystallization in HTMS. Uranium was chosen as an example, as it is a radioactive element with high metallic activity, which plays a critical role in the nuclear fuel cycle. Carrying out this experiment on uranium is more demanding than performing it on one of the rare or rare earth elements.

2. Experimental

Design and Fabrication of the DDE. Fig. 1(a) shows a schematic diagram and Fig. 1(b) a photograph of the DDE. The electrode consists of an upper and lower fastening screw rod (2) and nut (3) made of boron nitride, combined with a stainless-steel current collector (1) sealed with a corundum tube and a welded stainless-steel cylinder top fastener (4). The cathode disk (5) is sealed to form a simple mechanical structure which can easily be detached. The small hole (6) at the bottom of the nut (3) is used for contact with the electrolyte. The inner bottom surface of the nut (3) and the upper and lower sides of the cathode disk are both polished surfaces, which minimizes the gap between them. Fig. 1(c) presents the assembled DDE which is put into the high-temperature molten salt for 5 min and then withdrawn. After cooling, the nut is removed, and the cathode disk and the cylindrical salt ingot retained in the hole can be easily separated (Fig. 1d). No salt is observed on the inner bottom of the nut and the disassembled substrate also retains a shiny surface appearance (Fig. 1e), which makes characterization of the surface morphology and composition feasible and very convenient. Other experimental details are given in the Supporting Information.

3. Results and discussion

3.1. Electrochemical signal response of the DDE in a molten salt

Fig. 2 shows the CV curves collected on inert W, Mo, and GC, and (b) active Al, Ni, STS, and brass disks ($d = 3$ mm). Redox couples U^{4+}/U^{3+} (A/A′) and U^{3+}/U (C/C′) can be directly identified for inert W, Mo, and GC disk substrates, and have been widely verified on wire electrodes made from the same materials [30–34]. On the active Al, Ni, STS, and brass disk substrates, the signal of the U^{4+}/U^{3+} (A/A′) redox couple merges with the oxidation current of the disk due to the formation of alloys [30,35] and the easy oxidation of the material itself, resulting in different CV curves. Nevertheless, the CV signal response of the different substrates to the electrochemical reaction of uranium is identifiable and continuous, suggesting that although the electrode disk was only connected to the collector by direct contact rather than by welding, its conductivity is still excellent and there is no signal disconnection.

However, considering the harsh conditions of the HTMS system, it seems unfeasible to completely seal the DDE. In Fig. 2c, the current corresponding to the reduction peak of the U^{3+}/U (C/C′) redox couple was recorded at different times after the DDE had been inserted into the molten salt. In the initial 600 s, the current slowly decreased from 61.5 to 58 mA, and then remained stable for more than 1000 s before slowly increasing. One possible reason for this phenomenon may lie in the detachable design and hollow structure of the electrode package, which could contain some residual air inside the electrode or/and on the surface of the disk substrate inserted into the molten salt. The residual air would be physically heated and expand, which would slightly affect the active area of the disk. Nevertheless, the molten salt slowly permeated inside the electrode and dampened more of the electrode disk as expected, which caused an increase in the active area on the electrode and, subsequently, the cathodic current. Fortunately, for characterization of early nucleation and growth evolution, electrolysis experiments usually only focus on the initial seconds or tens of seconds. Therefore, the service life of an electrode used here to characterize electrodeposition in HTMS is undemanding. It is, however, not adequate for accurate electrochemical analyses such as those performed in the literature [1]. However, the DDE meets the requirements under our experimental conditions (the deposit sampling performance will be considered in the next section). Fig. 2d shows CA curves for electrocrystallization of U on a W disk electrode at various overpotentials in LiCl-KCl-3.2 wt% UCl_3 at 773 K. The dimensionless Scharifker–Hills model [36] fitting (Fig. S1 in the Supporting Information) suggests a big difference between the experimental data and the 3D growth of instantaneous and progressive models, which also has been observed in a bromide system [37]. In studies of lanthanides in the same chloride system, Pesic et al. [18,29,38] found that although the Scharifker–Hills models suggest a 3D mechanism for formation of nuclei, the SEM images of the initial morphology show 2D growth. The theoretical Scharifker-Hills models cannot fully reflect real nucleation and growth phenomena.

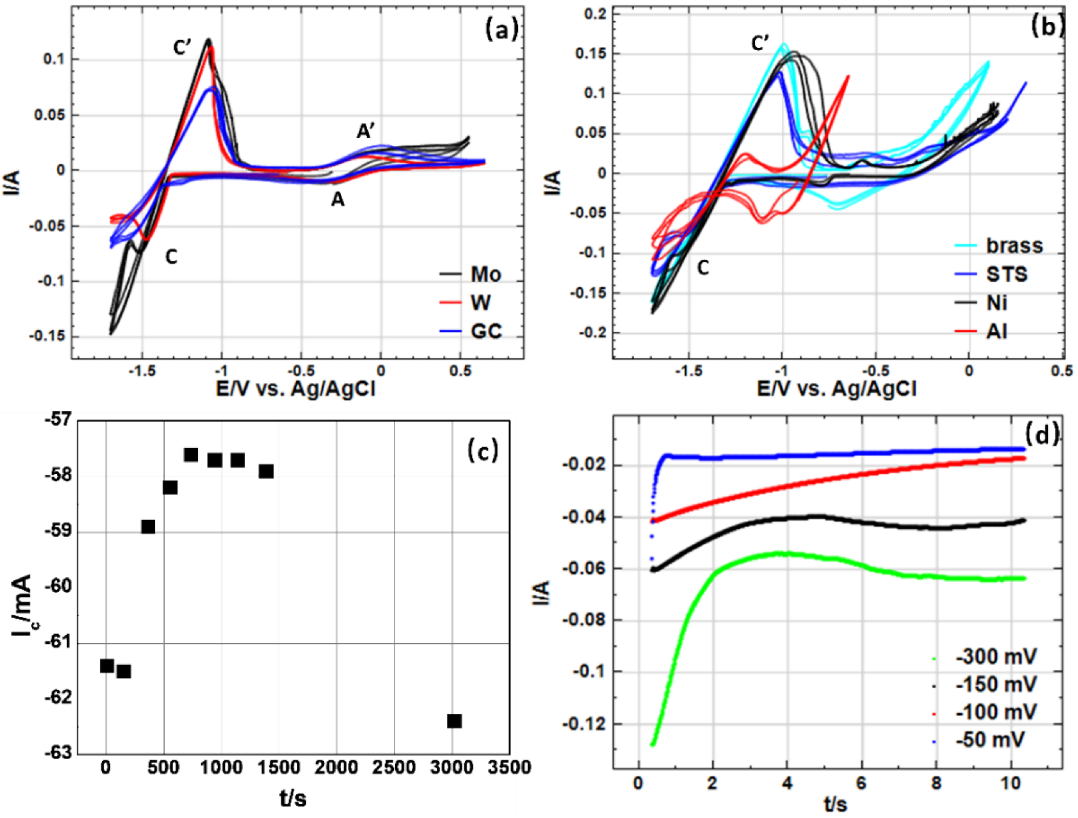

Fig. 2. CV curves of (a) inert W, Mo, GC and (b) active Al, Ni, STS, brass disks (d = 3 mm) in LiCl-KCl-3.2 wt% UCl_3 melt at 773 K; (c) The evolution of peak current (peak C) with time after the DDE was inserted in the melt; (d) CA curves for electrocrystallization of U on the W disk at various overpotentials in LiCl-KCl-10 wt% UCl_3 melt at 773 K.

3.2. *Sampling performance of uranium deposition and nucleation morphology on the DDE*

Fig. 3 presents low magnification SEM images and element mapping analyses for different disk substrates (GC, W, Mo, STS, Ni and Al). After removal of the solid salt (Fig. 1d), the residual salts on the various substrates were totally different. Based on the results of Cl mapping, there were small amounts of salt observed on the GC and W cathodes, and relatively more on the Mo, STS, Ni and Al electrodes. One possible reason for this diversity may lie in the surface smoothness of the substrate. Some scratches can be identified on the surfaces of all the manually-polished substrates except for the commercial GC cathode (Fig. S2 in the Supporting Information). Considering the STS, Ni and Al substrates, the deposited uranium can form an alloy with these substrates [30,39], which changes the physical surface and makes it rougher (Fig. S2 in the Supporting Information). Another reason might be the difference in properties between the materials themselves. The most convincing example is the Cl mappings of W and Mo substrates: both surfaces were scratched, but more salt was left on the Mo substrate than on the W substrate. In addition, the Al substrate also shows a positive tendency to form a very clean, uniform and dense alloy layer (Fig. S3 in the Supporting Information).

On the other hand, both Cl and U mappings suggest that the wettability of the melt on these substrates during the 60 s of electrolysis is mainly concentrated in the working area, except for the GC and STS electrodes. This phenomenon is consistent with the limited variation of peak current vs. time on the W substrate in the initial stage, as shown in Fig. 2c. When studying only the initial stage of nucleation and growth, the effect of molten salt infiltration on the actual working area is limited. Although the Cl mappings show that there is little salt on the W and GC substrates, the U mappings also suggest that smaller uranium deposits were retained on the GC and W surfaces. This implies that the uranium crystal sample was pulled off along with the solid salt. This phenomenon also appears in the morphology analysis of Nd nucleation on a Mo surface [38]. This can also be deduced from Cl and U mappings on the Mo substrate in Fig. 3, looking at the region where Cl is concentrated, and the signal of uranium is also relatively strong. Furthermore, the surface coverage rates of uranium on W and C were observed to be lower than on Mo cathodes after uranium dendrites had been scraped off in electrorefining tests [30,40]. Therefore, it can be considered that GC and W materials may be more conducive to the removal of the solid salts than the Mo substrate, leading to better characterization of initial nucleation.

Nevertheless, most of the active area of all the electrode substrates was not obviously stained nor covered with too much solid salt. Due to the surface homogeneity of the substrates, the characterization of uranium nucleation and crystal growth in these regions is still reasonable and representative. The initial deposition morphologies and corresponding EDS analyses on different substrates are presented in Figs. S4 and S5 in the Supporting Information. As an example, Fig. 4 shows SEM images of uranium nuclei deposited at −100 mV vs. U/U^{3+} on the GC disk substrate in different melt systems and with different electrolysis times. In particular, 1 wt% (Fig. 4a, d) or 10 wt% (Fig. 4b, c, e, f) UCl_3 melt systems were studied, and the electrolysis times were 2 s (Fig. 4b, e) or 10 s (Fig. 4a, d, c, f). In SEM images with low magnification (Fig. 4a–c), the distribution of clusters and a discrete form of uranium nuclei can be clearly identified without salt interference. On applying a greater magnification (Fig. 4d–f), clusters of uranium nuclei in the form of cubes or polyhedrons of different sizes are visible. However, K. Serrano et al. suggested a hemispherical nucleus based on a blurred SEM image on the GC substrate at −320 mV vs. U/U^{3+} in NaCl-KCl eutectic [26]. In addition, Fig. 5(a–d) shows the growth and evolution of uranium nuclei on the W substrate under various overpotentials and with different electrodeposition times. In the case of 100 mV

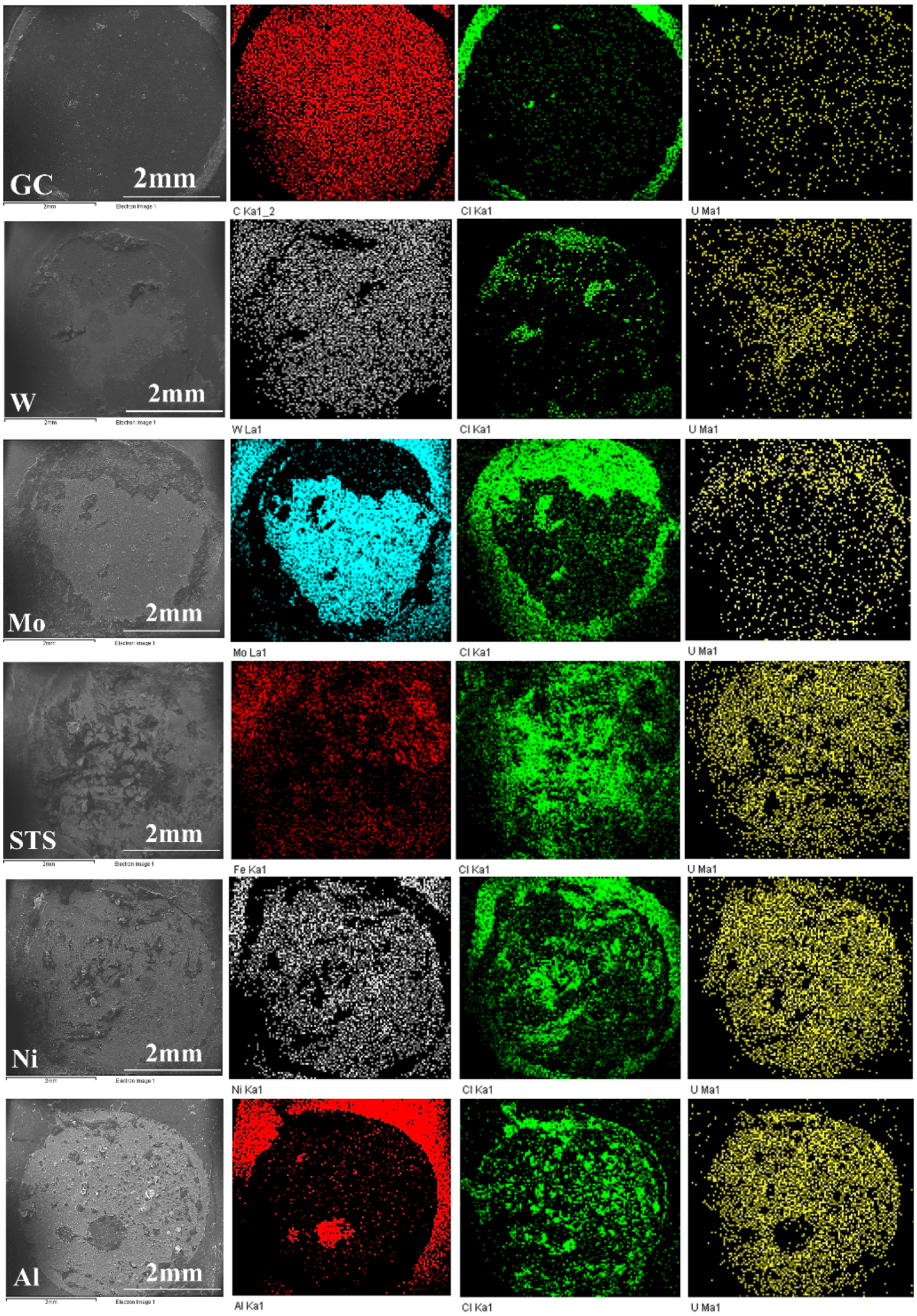

Fig. 3. SEM images and element mapping analyses of the uranium deposition site on different disk substrates ($d = 4$ mm) after deposition at -100 mV vs. U/U^{3+} for 60 s in LiCl-KCl-3.2 wt% UCl_3 at 773 K.

overpotential, the area covered by uranium nucleus growth did not change very much between 10 and 60 s. However, the size of the crystal nucleus grew with the increase in deposition time, and at 60 s, crystal nuclei were linked together to form a circular chain. These phenomena suggest the possible instantaneous nucleation of uranium. Fig. 5(e–h) show the uranium nuclei deposited after 10 s with different overpotential conditions (50, 100 and 150 mV, respectively). The coverage of uranium nuclei grew with increasing overpotential. At an overpotential of 150 mV (Fig. 5(g and h)), the uranium nuclei obtained at different sites of the same sample present different morphologies, showing that the crystal sample might be altered and pulled off along with the solid salt as mentioned above. Nevertheless, they present a similar arrangement and almost completely covered the tungsten substrate and even grew together. This phenomenon is generally observed in the electrodeposition of other metals [41]. The increase in overpotential reduces the size of the nuclei and increases their density. We can conclude that the initial nucleation and growth morphologies of uranium on GC and W can be successfully characterized using the DDE.

4. Conclusion

This work reports the design, construction, and electrochemical performance of a detachable disk electrode (DDE) for the characterization of initial nucleus growth and formation in HTMS electrodeposition. The aim was to solve the problem of deposit sampling where micro- or nano-sized nuclei are very sensitive to water and oxygen, accompanied by larger amount of solid salts. The DDE greatly reduces the complexity of experimental operation and ultimately enhances the effectiveness of the visual characterization of initial nucleation. It is successfully used to characterize the morphology of

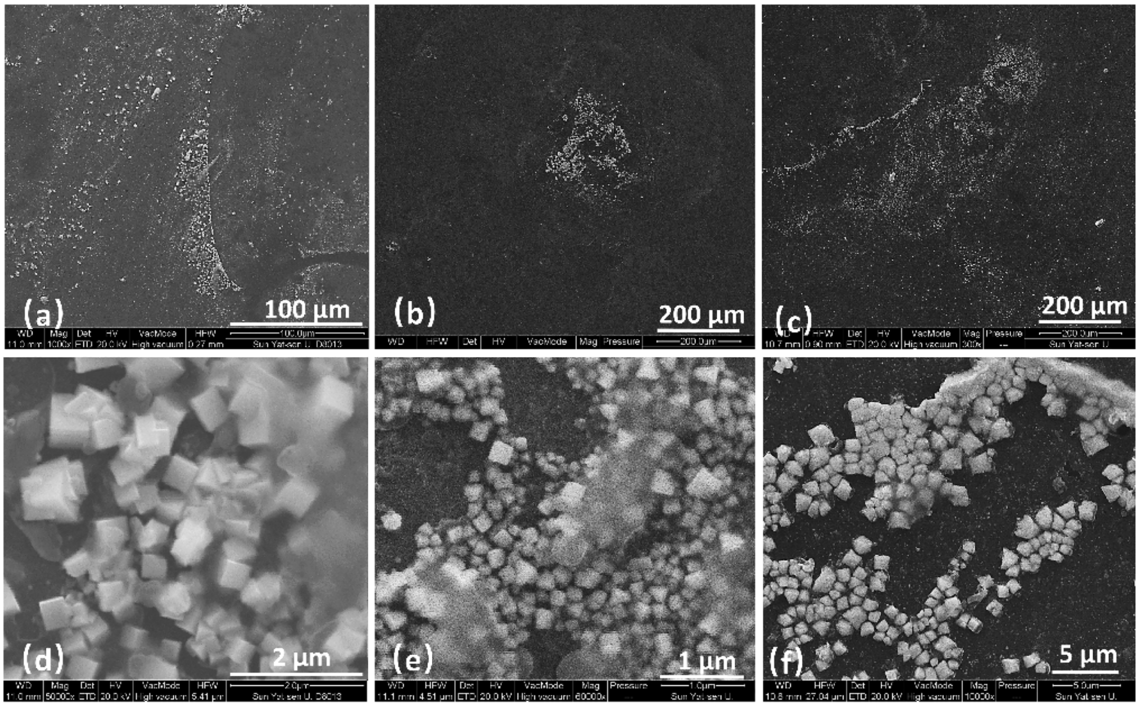

Fig. 4. SEM images of the initial nucleation of uranium deposited at −100 mV vs. U/U^{3+} on the GC disk substrate (d = 4 mm) in LiCl-KCl eutectic at 773 K. (a, d) for 10 s containing 1 wt% UCl$_3$, (b, e) after 2 s and (c, f) after 10 s containing 10 wt% UCl$_3$.

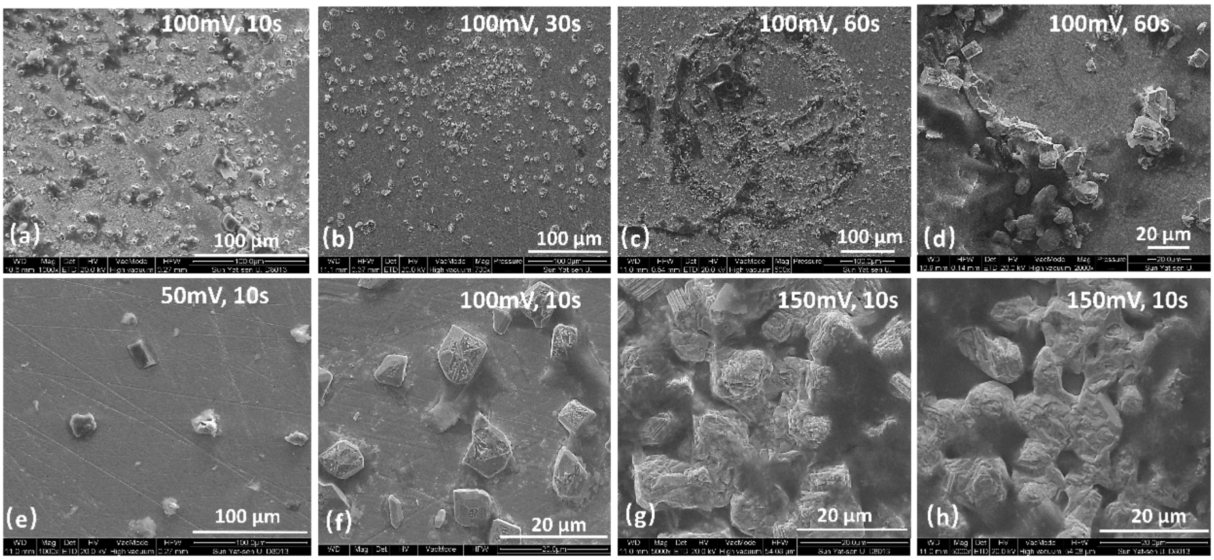

Fig. 5. SEM images of the initial nucleation and growth of uranium deposited on the W disk substrate (d = 5 mm) (a-d) after different times with the overpotential set at −100 mV vs. U/U^{3+}; and (e-h) using different overpotentials for 10 s in LiCl-KCl eutectic containing 10 wt% UCl$_3$ at 773 K.

uranium nucleation and growth on different substrates. The proposed DDE provides a facile scheme with wide applications to the visual characterization of initial nucleation in high temperature molten salt electrodeposition.

CRediT authorship contribution statement

Kui Liu: Conceptualization, Investigation, Methodology, Visualization, Validation, Data curation, Funding acquisition, Writing - original draft. **Yue Ma:** Software, Formal analysis, Writing - review & editing. **Mingliang Kang:** Funding acquisition, Supervision, Writing - review & editing. **Biao Wang:** Project administration, Supervision.

Acknowledgements

This work was financially supported by the National Postdoctoral Program for Innovative Talents (No. BX20180387) and the China Postdoctoral Science Foundation Grant (2019M653182), the National Natural Science Foundation of China (NSFC, No. 51904360 and 41773095) and the Young Teacher Foundation of Sun Yat-sen University (No. 191gpy293).

Appendix A. Supplementary data

Supplementary data to this article can be found online at https://

doi.org/10.1016/j.elecom.2020.106780.

References

[1] D.K. Corrigan, E.O. Blair, J.G. Terry, A.J. Walton, A.R. Mount, Enhanced electroanalysis in lithium potassium eutectic (LKE) using microfabricated square microelectrodes, Anal. Chem. 86 (2014) 11342–11348.

[2] S.A. Kuznetsov, Electrochemical techniques——some aspects of electrochemical behaviour of refractory metal complexes, in: M. Gaune-Escard (Ed.), Molten Salts: From Fundamentals to Applications, Springer Netherlands, Dordrecht, 2002, pp. 283–303.

[3] K. Grjotheim, C. Krohn, M. Malinovsky, K. Matiasovsky, J. Thonstad, Aluminum Electrolysis: The Chemistry of the Hall-Heroult Process, Aluminium-Verlag GmbH, Dusseldorf, Germany, 1977.

[4] G.J. Kipouros, D.R. Sadoway, The electrodeposition of improved molybdenum coatings from molten salts by the use of electrolyte additives, J. Appl. Electrochem. 18 (1988) 823–830.

[5] F. Mansfeld, F. Perez, Surface modification of Al/15% SiC metal matrix composite in molten salts containing $CeCl_3$, Surf. Coat. Technol. 86 (1996) 449–453.

[6] S.K. Cho, F.R.F. Fan, A.J. Bard, Electrodeposition of crystalline and photoactive silicon directly from silicon dioxide nanoparticles in molten $CaCl_2$, Angew. Chem. Int. Ed. 51 (2012) 12740–12744.

[7] D.R. Sadoway, The electrochemical processing of refractory metals, J. Min. Metal. Mater. Soc. 43 (1991) 15–19.

[8] R.O. Suzuki, T. Matsunaga, K. Ono, T.N. Harada, T.N. Deura, Titanium powder prepared by magnesiothermic reduction of Ti^{2+} in molten salt, Metall. Mater. Trans. B 30 (1999) 403–410.

[9] S.X. Li, T.A. Johnson, B.R. Westphal, K.M. Goff, R.W. Benedict, Electrorefining experience for pyrochemical reprocessing of spent EBR-II driver fuel, Idaho Natl. Lab. (INL) (2005).

[10] T. Koyama, M. Iizuka, Pyrochemical fuel cycle technologies for processing of spent nuclear fuels: Developments in Japan, Reprocessing and Recycling of Spent Nuclear Fuel, Elsevier, 2015, pp. 457–519.

[11] H.-S. Lee, G.-I. Park, K.-H. Kang, J.-M. Hur, J.-G. Kim, D.-H. Ahn, Y.-Z. Cho, E.-H. Kim, Pyroprocessing technology development at KAERI, Nucl. Eng. Tech. 43 (2011) 317–328.

[12] B.Y. Kim, J.-I. Yun, Temperature effect on fluorescence and UV–vis absorption spectroscopic properties of Dy(III) in molten LiCl–KCl eutectic salt, J. Lumin. 132 (2012) 3066–3071.

[13] I.B. Polovov, V.A. Volkovich, J.M. Charnock, B. Kralj, R.G. Lewin, H. Kinoshita, I. May, C.A. Sharrad, In situ spectroscopy and spectroelectrochemistry of uranium in high-temperature alkali chloride molten salts, Inorg. Chem. 47 (2008) 7474–7482.

[14] J. Young, J. White, High-temperature cell assembly for spectrophotometric studies of molten fluoride salts, Anal. Chem. 31 (1959) 1892–1895.

[15] A. Merwin, W.C. Phillips, M.A. Williamson, J.L. Willit, P.N. Motsegood, D. Chidambaram, Presence of Li clusters in molten LiCl-Li, Sci. Rep. 6 (2016) 25435.

[16] C. Malherbe, G. Eppe, B. Gilbert, Determination of the Al_2O_3 content in $NaF–AlF_3–CaF_2–Al_2O_3$ melts at 950 °C by Raman spectroscopy, Anal. Chem. 86 (2014) 8073–8081.

[17] C.A. Schroll, S. Chatterjee, T.G. Levitskaia, W.R. Heineman, S.A. Bryan, Electrochemistry and spectroelectrochemistry of europium (III) chloride in 3LiCl–2KCl from 643 to 1123 K, Anal. Chem. 85 (2013) 9924–9931.

[18] H. Tang, B. Pesic, Electrochemical behavior of $LaCl_3$ and morphology of La deposit on molybdenum substrate in molten LiCl–KCl eutectic salt, Electrochim. Acta 119 (2014) 120–130.

[19] J. Phillips, R. Gale, R. Wier, R. Osteryoung, Glassy carbon rotating ring-disc electrode for molten salt studies, Anal. Chem. 48 (1976) 1266–1268.

[20] G. Wei, X. Liu, Y. Lu, Z. Wang, S. Liu, G. Ye, J. Chen, Microplasma anode meeting molten salt electrochemistry: charge transfer and atomic emission spectral analysis, Anal. Chem. 90 (2018) 13163–13166.

[21] S. Natsui, T. Sudo, T. Kikuchi, R.O. Suzuki, Morphology of lithium droplets electrolytically deposited in $LiCl–KCl–Li_2O$ melt, Electrochem. Commun. 81 (2017) 43–47.

[22] Y.T. Jee, M. Park, S. Cho, J.-I. Yun, Selective morphological analysis of cerium metal in electrodeposit recovered from molten LiCl-KCl eutectic by radiography and computed tomography, Sci. Rep. 9 (2019) 1346.

[23] M. Tylka, J. Willit, M. Williamson, Electrochemical nucleation and growth of uranium and plutonium from molten salts, J. Electrochem. Soc. 164 (2017) H5327–H5335.

[24] A.-L. Bieber, L. Massot, M. Gibilaro, L. Cassayre, P. Taxil, P. Chamelot, Silicon electrodeposition in molten fluorides, Electrochim. Acta 62 (2012) 282–289.

[25] M. Bermejo, J. Gomez, A. Martinez, E. Barrado, Y. Castrillejo, Electrochemistry of terbium in the eutectic LiCl–KCl, Electrochim. Acta 53 (2008) 5106–5112.

[26] K. Serrano, P. Taxil, Electrochemical nucleation of uranium in molten chlorides, J. Appl. Electrochem. 29 (1999) 505–510.

[27] K. Carleton, J. Olson, A. Kibbler, Electrochemical nucleation and growth of silicon in molten fluorides, J. Electrochem. Soc. 130 (1983) 782–786.

[28] G. Gunawardena, G. Hills, I. Montenegro, B. Scharifker, Electrochemical nucleation: part I. General considerations, J. Electroanal. Chem. 138 (1982) 225–239.

[29] H. Tang, B. Pesic, Electrochemistry of $ErCl_3$ and morphology of erbium electrodeposits produced on Mo substrate in early stages of electrocrystallization from LiCl–KCl molten salts, Electrochim. Acta 133 (2014) 224–232.

[30] C.H. Lee, T.-J. Kim, S. Park, S.-J. Lee, S.-W. Paek, D.-H. Ahn, S.-K. Cho, Effect of cathode material on the electrorefining of U in LiCl-KCl molten salts, J. Nucl. Mater. 488 (2017) 210–214.

[31] K. Liu, H.B. Tang, J.W. Pang, Y.L. Liu, Y.X. Feng, Z.F. Chai, W.Q. Shi, Electrochemical properties of uranium on the liquid gallium electrode in LiCl-KCl eutectic, J. Electrochem. Soc. 163 (2016) D554–D561.

[32] D.S. Maltsev, V.A. Volkovich, E.N. Vladykin, B.D. Vasin, An electrochemical study of uranium (III) and (IV) species in fused alkali chlorides, ECS Trans. 64 (2014) 357–367.

[33] R.O. Hoover, M.R. Shaltry, S. Martin, K. Sridharan, S. Phongikaroon, Electrochemical studies and analysis of 1–10 wt% UCl_3 concentrations in molten LiCl–KCl eutectic, J. Nucl. Mater. 452 (2014) 389–396.

[34] P. Masset, D. Bottomley, R. Konings, R. Malmbeck, A. Rodrigues, J. Serp, J.P. Glatz, Electrochemistry of uranium in molten LiCl-KCl eutectic, J. Electrochem. Soc. 152 (2005) A1109–A1115.

[35] L. Cassayre, C. Caravaca, R. Jardin, R. Malmbeck, P. Masset, E. Mendes, J. Serp, P. Soucek, J.P. Glatz, On the formation of U-Al alloys in the molten LiCl-KCl eutectic, J. Nucl. Mater. 378 (2008) 79–85.

[36] B. Scharifker, G. Hills, Theoretical and experimental studies of multiple nucleation, Electrochim. Acta 28 (1983) 879–889.

[37] H. Tang, Y. Du, Y. Li, M. Wang, H. Wang, Z. Yang, B. Li, R. Gao, Electrochemistry of UBr 3 and preparation of dendrite-free uranium in LiBr-KBr-CsBr eutectic melts, J. Nucl. Mater. 508 (2018) 403–410.

[38] H. Tang, B. Pesic, Electrochemistry and the mechanisms of nucleation and growth of neodymium during electroreduction from LiCl–KCl eutectic salts on Mo substrate, J. Nucl. Mater. 458 (2015) 37–44.

[39] L. Cassayre, C. Caravaca, R. Jardin, R. Malmbeck, P. Masset, E. Mendes, J. Serp, P. Soucek, J.-P. Glatz, On the formation of U-Al alloys in the molten LiCl–KCl eutectic, J. Nucl. Mater. 378 (2008) 79–85.

[40] J.-H. Lee, Y. Kang, S. Hwang, J. Shim, E. Kim, S. Park, Application of graphite as a cathode material for electrorefining of uranium, Nucl. Technol. 162 (2008) 135–143.

[41] T. Vargas, D. Inman, Controlled nucleation and growth in chromium electroplating from molten LiCl-KCl, J. Appl. Electrochem. 17 (1987) 270–282.